NASA SP-330

APOLLO 17

Preliminary Science Report

PREPARED BY

LYNDON B. JOHNSON SPACE CENTER

Scientific and Technical Information Office 1973

NATIONAL AERONAUTICS AND SPACE ADMINISTRATION

Washington, D.C.

15. Surface Electrical Properties Experiment

Gene Simmons,[a†] *David Strangway,*[b‡] *Peter Annan,*[c] *Richard Baker,*[a]
Lawrence Bannister,[a] *Raymon Brown,*[a] *William Cooper,*[a] *Dean Cubley,*[b]
Joseph deBettencourt,[d] *Anthony W. England,*[e‡] *John Groener,*[a] *Jin-Au Kong,*[a]
Gerald LaTorraca,[a] *James Meyer,*[a] *Ved Nanda,*[a] *David Redman,*[c]
James Rossiter,[c] *Leung Tsang,*[a] *Joseph Urner,*[d] *and Raymond Watts*[c]

The surface electrical properties (SEP) experiment was used to explore the subsurface material of the Apollo 17 landing site by means of electromagnetic radiation. The experiment was designed to detect electrical layering, discrete scattering bodies, and the possible presence of water. From the analysis of the data, it was expected that values of the electrical properties (dielectric constant and loss tangent) of lunar material in situ would be obtained.

The SEP experiment is important for several reasons. First, the values of the electrical properties of the outer few kilometers of rock and soil of the Moon, measured in situ for the first time, may help others interpret many observations already made with both Earth-based and lunar orbital bistatic radar. Second, the SEP experiment will provide data that are needed to interpret the observations made with the lunar sounder, an Apollo 17 orbital experiment. In the Apollo lunar sounder experiment, the time intervals required for electromagnetic waves to penetrate the Moon, be reflected, and return to the surface of the Moon were measured. Of more interest than times, however, are depths, which can be obtained from the lunar sounder delay times and the dielectric constant that is measured in the SEP experiment. Third, the results of the SEP experiment are expected to help define the stratigraphy of the Apollo 17 landing site. Visual observations made by the crewmen and recorded with cameras are restricted to the surface of the Moon. The SEP experiment will extend to depth those visual observations made at the surface and perhaps reveal features at depth that do not reach the surface.

[a]Massachusetts Institute of Technology.
[b]NASA Lyndon B. Johnson Space Center.
[c]University of Toronto.
[d]Raytheon Company.
[e]U.S. Geological Survey.
[†]Principal Investigator.
[‡]Coinvestigator.

DESCRIPTION OF THE EXPERIMENT

The basic principle of the SEP experiment is interferometry. This principle involves only the interference of two or more waves to produce an interference pattern. The inversion of the interference pattern in terms of the spatial distribution of the electrical properties is the basic aim of the experiment (fig. 15-1). The experiment is most easily understood in terms of a single dipole antenna for radiating electromagnetic energy and a loop receiver for measuring the magnitudes of the fields. In the

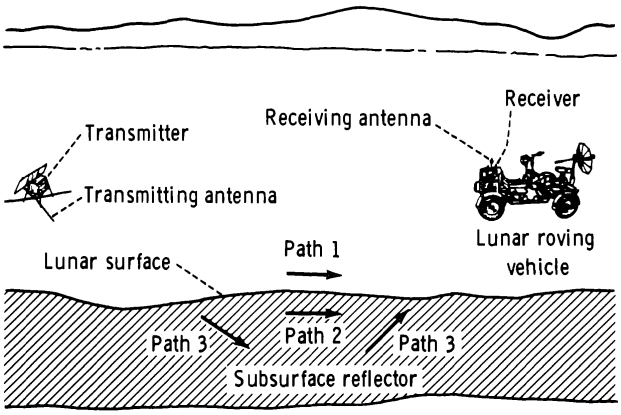

FIGURE 15-1.–Simplified schematic diagram of the SEP experiment. Electromagnetic radiation from the transmitting dipole antenna travels along path 1 (above the surface), along path 2 (below the surface), and, if reflectors are present, along path 3.

early developmental stages of this experiment, exactly this configuration was used (ref. 15-1).

The electromagnetic energy radiated from the transmitting antenna travels along various paths. In the "half-space" case, one wave travels above the interface through "free" space and another travels below the interface through subsurface material. Because the velocity of electromagnetic waves in a solid medium is different from that in free space, the two waves interfere and produce a distinctive interference pattern. This case has been studied extensively from both experimental and theoretical viewpoints since 1909 (ref. 15-2). The correct mathematical solutions, although somewhat complicated, are now well known (ref. 15-3). An example of a theoretical interference pattern for the half-space case is shown in figure 15-2. The spacing between successive maximums or successive minimums is related to the frequency of the wave and to the dielectric constant of the medium, and the rate at which the field strength decreases with distance is related to the loss tangent of the medium. This type of pattern is present in some of the lunar data.

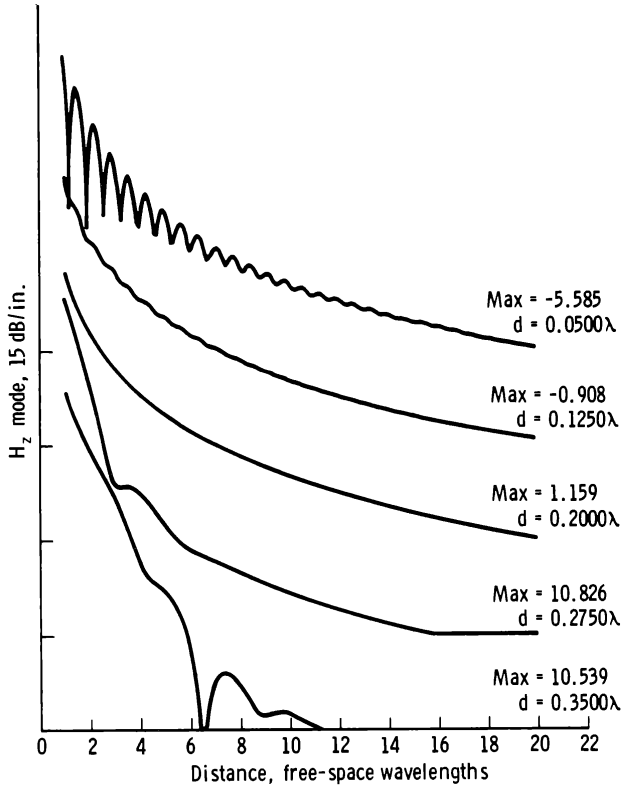

FIGURE 15-2.–Theoretical interference pattern for a half-space case, in which medium 1 is solid and medium 2 is free space; where depth $d = 0$, medium 1 loss tangent $p_1 = 0.0300$, medium 2 loss tangent $p_2 = \infty$, medium 2 dielectric constant $\epsilon_{r_2} = \infty$, and frequency $f = 299.8$ MHz. The symbol H_z represents the vertical component of the magnetic field. The points on the ordinate indicate the maximum (max) values of each wave pattern.

If a reflecting horizon occurs at depth, such as the case shown schematically in figure 15-1, then a reflected wave will interfere at the surface of the medium with the other waves. Figure 15-3 is a theoretical curve showing the distinct interference pattern produced by a reflected wave. The presence of additional reflecting horizons in the subsurface would produce still more complicated interference patterns.

In the Apollo 17 SEP experiment, two crossed dipole antennas that radiated sequentially were used. In addition, several frequencies–1, 2.1, 4, 8.1, 16, and 32.1 MHz–were used. Because each transmitting antenna radiates at each frequency for a sufficiently long time, the experiment results can be analyzed in terms of continuous waves. The shortest sampling time at the lowest frequency includes approximately 33 000 cycles.

THEORETICAL BASIS

The SEP experiment is the first geophysical field technique to use the dielectric properties of rocks rather than the conductive properties. In that sense, the experiment is entirely new. Consequently, all the

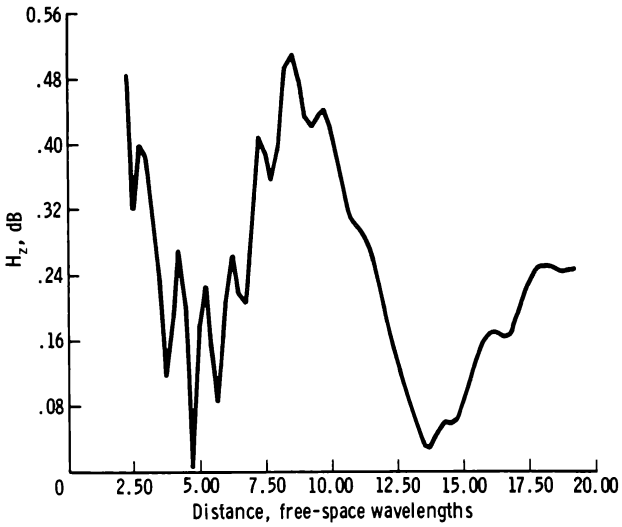

FIGURE 15-3.–Theoretical curve for the case of a single layer over a reflector. The layer is four free-space wavelengths ($4\lambda_0$) thick (ref. 15-8).

experimental techniques and most of the theoretical basis have been developed specifically for the lunar experiment. Descriptions of the early versions (circa 1968) of the technique are given in references 15-1, 15-4, and 15-5. In this report, the physical and mathematical basis of the experiment is outlined and the discussions in references 15-6 to 15-8 are followed. Theoretical work has been limited to the electric and magnetic fields that result from dipole antennas on plane, horizontal, layered media. For mathematical details, the reader is referred to the original sources.

In the theoretical development, consideration is given first to electromagnetic propagation in an unbounded, homogeneous, isotropic dissipative medium and next to propagation near the plane interface of two semi-infinite homogeneous media (specialized to a lossy dielectric below an empty (or free) space region, popularly called the half-space case). Then, the effects of inhomogeneous horizontal stratification are considered, specialized initially to a lossy dielectric region of two layers, the first of depth d and the second of infinite depth and having electrical properties differing from the adjacent layer and the semi-infinite space above.

UNBOUNDED, HOMOGENEOUS, LOSSY DIELECTRIC MEDIA

Electromagnetic propagation in unbounded dissipative media is treated adequately in references 15-3 and 15-9 to 15-13. Variation of electric and magnetic fields with time t is usually expressed as $\exp(j\omega t)$ where the rotative operator $j = \sqrt{-1}$ and the radian frequency $\omega = 2\pi f$ (where the frequency f is expressed in hertz); this exponential is hereafter suppressed. Meter-kilogram-second units are used where, in vacuo, the dielectric constant or permittivity $\epsilon_0 = 1 \times 10^{-9}/36\pi$ F/m and the permeability $\mu_0 = 4\pi \times 10^{-7}$ H/m. The phase velocity in vacuo is $c = 1/\sqrt{\mu_0 \epsilon_0} = 3 \times 10^8$ m/sec. Mathematically, the field expressions are solutions to Maxwell's equations.

The dissipative medium is characterized by its electrical constants, real relative dielectric constant ϵ_r and conductivity σ (mho/m). (For a vacuum, $\epsilon_r = 1$.) The media are customarily considered to be nonmagnetic with permeability $\mu = \mu_0$. The finite value of σ gives rise to a complex relative dielectric constant ϵ_r', a complex refractive index N, and a complex phase constant $k = \beta - j\alpha$ where β is the phase constant and α is the attenuation constant. A typical component of electric field E at a large distance R from the radiating source varies with R according to

$$E = E_0 e^{-jkR} = E_0 e^{-\alpha R} e^{-j\beta R} \tag{15-1}$$

where E_0 is a reference value of E (independent of R).

The complex relative dielectric constant is

$$\epsilon_r' = \epsilon_r(1 - jp) = \epsilon_r - jx \tag{15-2}$$

where p is the loss tangent

$$p = \frac{\sigma}{\omega \epsilon_0 \epsilon_r} = 60\sigma \frac{\lambda_0}{\epsilon_r} \tag{15-3}$$

with λ_0 the free-space wavelength in meters.

The refractive index relative to vacuum is

$$N = \sqrt{\epsilon_r'} = \sqrt{\epsilon_r}(1 - jp)^{1/2} \tag{15-4}$$

The evaluation of the complex radical may be accomplished by the 50-yr-old method of G. W. Pierce (ref. 15-14), recently revived by King (ref. 15-9), as follows.

$$\sqrt{1 - jp} = f(p) - jg(p) \tag{15-5}$$

where

$$f(p) = \cosh\left(\frac{1}{2}\sinh^{-1} p\right) = \left[\frac{1}{2}\left(\sqrt{1 + p^2} + 1\right)\right]^{1/2}$$

$$g(p) = \sinh\left(\frac{1}{2}\sinh^{-1} p\right) = \left[\frac{1}{2}\left(\sqrt{1 + p^2} - 1\right)\right]^{1/2}$$

Thus, the complex phase constant k may be written as

$$k = \beta - j\alpha = \beta_0\sqrt{\epsilon_r'} = \beta_0 N = \beta_0\sqrt{\epsilon_r}[f(p) - jg(p)] \tag{15-6}$$

where the phase constant (real) in vacuo $\beta_0 = 2\pi/\lambda_0 = \omega\sqrt{\mu_0 \epsilon_0}$. Hence

$$\left.\begin{aligned} \beta &= \beta_0\sqrt{\epsilon_r} f(p), \text{ rad/m} \\ \lambda &= \frac{3 \times 10^8}{f}, \text{ m} \\ \alpha &= \beta_0\sqrt{\epsilon_r}\, g(p), \text{ Np/m} \end{aligned}\right\} \tag{15-7}$$

When the loss tangent p is small, say $p < 0.5$, then $f(p) = 1$ and $g(p) = p/2$; this is the case encountered in the lunar SEP experiment, so that

$$\left.\begin{aligned} \beta &= \beta_0\sqrt{\epsilon_r} = \frac{2\pi}{\lambda}, \text{ rad/m} \\ \lambda &= \frac{\lambda_0}{\sqrt{\epsilon_r}}, \text{ m} \\ \alpha &= \frac{60\pi\sigma}{\sqrt{\epsilon_r}}, \text{ Np/m} \\ &= 1.64\,\frac{\sigma}{\sqrt{\epsilon_r}}, \text{ dB/km} \end{aligned}\right\} \quad (15\text{-}8)$$

and α is independent of frequency. If σ and ϵ_r are constant with frequency, then p is proportional to f; if p is constant with f, then σ/ϵ_r is proportional to f.

Propagation in Layered Media

For propagation in semi-infinite space near and above a semi-infinite, homogeneous (nonlayered) lossy dielectric, see references 15-3, 15-9, 15-10, and 15-15 to 15-17. References 15-16 and 15-17 are especially useful for layered media. Earlier application was to ground-wave propagation along the surface of the Earth, generally where the loss tangent of the Earth is large. The mathematical solutions are involved; they were solved initially by Sommerfeld in 1909 (ref. 15-2) with later (1926) correction of the famous $\sqrt{-1}$ sign error (ref. 15-18). A complete history, with proof of the existence of Sommerfeld's controversial surface wave, is given by Baños (ref. 15-3). The resulting field equations (for electric field E and magnetic field H) depend on the nature of the source. In theory, there are four source dipoles: the horizontal electric dipole (HED) and vertical electric dipole (wires), the horizontal magnetic dipole, and the vertical magnetic dipole (VMD). In the SEP experiment, a tuned series of wire antenna radiators (thus extensions of the elemental HED) is used, and the cylindrical coordinate values of magnetic field H_ρ, H_ϕ, and H_z are measured.

The major difference in typical ground-wave propagation from that on the Moon (or in earthbound glaciers and deserts) is in the low values of ϵ_r and p for the latter. For the case of a semi-infinite Moon below semi-infinite space, the solution is that for the so-called half-space case; the integral method of solution (ref. 15-3) involves general integrals of the type

$$I(a,b,r) = \int_{-\infty}^{\infty} F(\lambda)e^{-\gamma_1 a-\gamma_2 b}H_0^1(\lambda r)\lambda\, d\lambda \quad (15\text{-}9)$$

where the function $F(\lambda)$ is devoid of exponential behavior, H_0^1 is the zero-order Hankel function of the first kind, and $\gamma_i = (\lambda^2 - k_i^2)^{1/2}$ may be called a complex propagation factor ($i = 1$ denoting the lunar soil and $i = 2$ the space above). The variable λ used in equations (15-9) and (15-10) is a complex separation (or eigen) variable of integration and should not be confused with the wavelength.

In a cylindrical coordinate system with the source dipole at a height h above the origin of the coordinates (ρ, ϕ, z), two essential integrals $U(a,b,r)$ and $V(a,b,r)$ are required to determine the vector potential Π from which the fields E and H are derived. The relationship of E and H is derived from Maxwell's equations and continuity relations at the space-dielectric plane boundary ($z = 0$). The U and V integrals differ in the value of $F(\lambda)$ used; thus, for the V integral

$$F(\lambda) = \frac{k_1^2\gamma_2 - k_2^2\gamma_1}{\left(k_1^4 - k_2^4\right)\left(\lambda^2 - k_0^2\right)} \quad (15\text{-}10)$$

where

$$\left.\begin{aligned} k_0^2 &= \frac{k_1^2}{N^2 + 1} \\ N &= \frac{k_1}{k_2} = \frac{k_i}{\beta_0} = \sqrt{\epsilon'_{r_1}} \end{aligned}\right\} \quad (15\text{-}11)$$

In equation (15-11), the refractive index N (eq. (15-4)) is the reciprocal of n used by Baños (ref. 15-3) and others.

For evaluating a component of the magnetic field (e.g., H_z) in the SEP experiment, the U integral is required (actually the partial derivative of U). Here, $a = 0$, $b = h + z$, and the exponential involving a in equation (15-9) is unity; thus, U is written as $U(0,b,r)$. If $h = 0$, then U becomes $U(0,z,r)$.

The integral solution involves, generally, saddle-

point or double-saddle-point approximation methods (ref. 15-3). However, if $h = z = 0$, the solution for $U(0,0,r)$ is exact, as found by Van der Pol. Thus, the expressions for H_z waves broadside to the horizontal wire (HED) are exact as are those for the tangential component of electric field E_ϕ (VMD) (first noted by Wait (ref. 15-16)). If h or z (or both) are nonzero values, approximate methods must be used; these methods are very laborious because complex contour integration must be used with consequent studies of poles and branch cuts in the integrals $I(a,b,r)$.

The resulting field expression for the half-space case consists of two components, one a wave traveling above the surface with the phase velocity of space and the second a lateral wave; these two waves interfere. An example is shown in figure 15-2 for H_z lateral waves broadside to an HED for several values of ϵ_{r_1} and $p_1 = 0.03$. The lateral wave is that component of energy traveling in the dielectric but refracting across the boundary to reach the receiver at height $h = z$.

For typical terrestrial soils, the loss tangent p of the ground is so high that the lateral wave is relatively too small to be observed. However, in glaciers, polar regions, and deserts, such interference patterns as those shown in figure 15-3 may be observed.

Horizontal Stratification

Two Layers.—Wave propagation in stratified regions has been treated generally by Brekhovskikh (ref. 15-17) and Wait (ref. 15-16); the properties of antennas in such regions have been discussed by Galejs (ref. 15-15). As specified for the SEP experiment, the previously mentioned treatments in references 15-6 and 15-8 find useful application. The geometry is that of figure 15-4. The solutions are

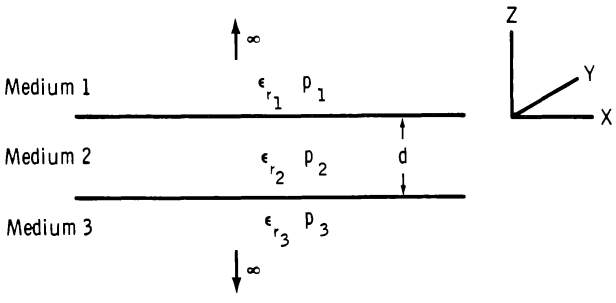

FIGURE 15-4.—Geometry for the case of a single layer over a half space. Medium 1, $a \geq 0$ (free space); medium 2, $-h \leq z \leq 0$; medium 3, $a < -h$.

integrals, similar to equation (15-9). The theoretical problem is reduced to that of solving the integrals. Three techniques have been used: (1) numerical integration on a digital computer, (2) asymptotic expansions that lead to geometrical optics approximations, and (3) contour integration to yield a normal mode solution (mode). In the geometrical optics approximation (GOA) method, the resulting field at the receiver consists of the space and lateral wave components (the half-space case) plus those attributable to reflections from the boundary between the upper layer of thickness d and the lower semi-infinite layer. (Lateral waves at this boundary and their effects have been generally neglected.) The formulation of reflections is approximate, but the GOA solution is considered satisfactory if the depth d is greater than the wavelength λ in the upper layer. An example is shown in figure 15-3, where $d = 4\lambda_0$, for lateral waves broadside to an HED. In the mode approach, the contributions to the integrals are identified in terms of the normal modes of wave propagation.

Multiple Layers.—Solutions to the various integrals (eq. (15-9)) for multiple layers can also be obtained by numerical integration and by using normal mode theory. The numerical integration method (refs. 15-8 and 15-19) provides quite exact solutions but requires much computer time; however, the method provides a check on other techniques and can be extended readily to large numbers of layers. In the GOA method, the problem is treated in terms or rays (thus, distances must be large compared with various wavelengths); therefore, solutions that are readily interpretable against a background of physical optics are provided. Unfortunately, the GOA is invalid for "thin" layers, the case for both glaciers and the Moon for at least some of the SEP experiment frequencies. The formulation and solutions for certain parameters are given in references 15-6 and 15-8. The theoretical curve for one set of parameters is shown in figure 15-5. The lack of agreement between the GOA and the numerical integration at distances less than 7λ is caused by the approximations in the GOA and indicates clearly that the proper solution must be chosen for a particular experimental situation. The normal mode solution, valid for thin layers such as appear to be present at the Apollo 17 site, was formulated by Tsang, Kong, and Simmons (ref. 15-8).

We are rather sure that our various formulations of the solution are correct. These formulations have

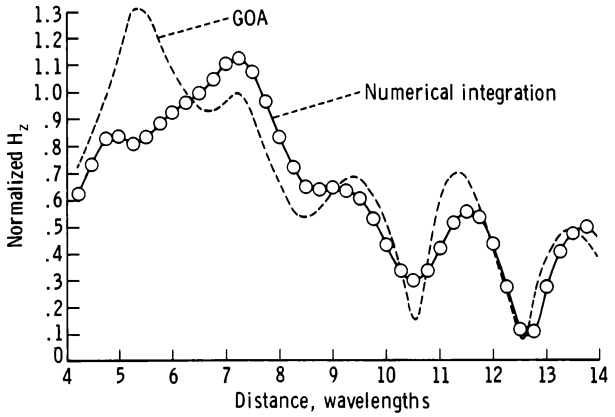

FIGURE 15-5.–Comparison of the geometrical optics approximation (dashed curve) with the Tsang exact solution (solid curve), obtained by numerical integration, for a single-layer case (ref. 15-8). Note the excellent agreement for all peaks except the first.

been tested against field data collected on glaciers for which the geometry was known from previous investigations using such other techniques as seismic, gravity, and drilling (refs. 15-1, 15-8, and 15-20). They have also been tested against laboratory data obtained with analog scale models.

The antenna radiation patterns of both the receiving loops and the transmitting dipoles are important in the analysis of the lunar data. The theoretical patterns for the transmitting antenna have been calculated (ref. 15-21), and the results are shown in figure 15-6. It has not been possible to calculate, with equal confidence, the patterns for the receiving antennas because of the effects of the lunar roving vehicle (LRV). From the data obtained on the Moon, however, it is deduced that the influence on the H_z component is minimal; thus, our preliminary data analysis is based on that component. In order to interpret the H_ρ and H_ϕ components, the effect of the radiation pattern of the receiving antenna must be removed.

THE EQUIPMENT

On the Moon, the crewmen deployed a small, low-power transmitter (fig. 15-7) and laid on the surface two crossed dipole antennas that were 70 m long tip to tip. The receiver and receiving antennas, shown in figure 15-8, were mounted on the LRV. Inside the receiver, there was a tape recorder which recorded the data on magnetic tape. The entire tape recorder, the data storage electronics assembly (DSEA), was returned to Earth. In addition to the

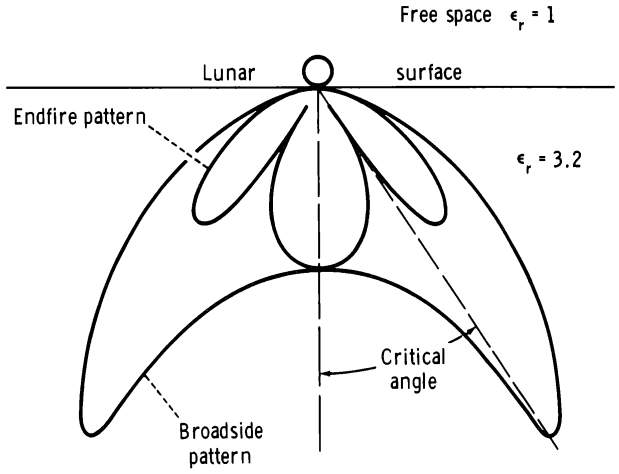

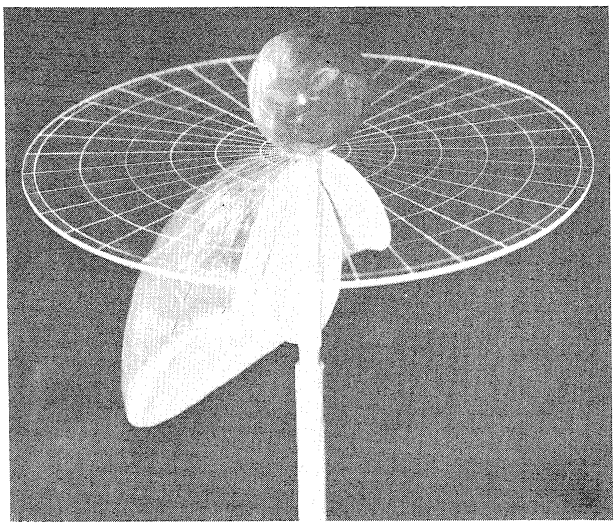

FIGURE 15-6.–Model of the theoretical radiation pattern for the SEP experiment transmitting antenna on the Moon (ref. 15-22). (a) Diagram. (b) Photograph.

SEP experiment data, information on the location of the LRV, obtained from the LRV navigation system, was also recorded on the tape.

Description

The electromagnetic radiation at the six SEP experiment frequencies is transmitted and received according to the scheme shown in figure 15-9. One data frame, which is 38.4 sec in duration, consists of six 6.4-sec subframes that are identical except for the receiver calibration and synchronization process. In subframe 1, for example, the receiver is calibrated at 32.1 and 16 MHz and the synchronization signal is

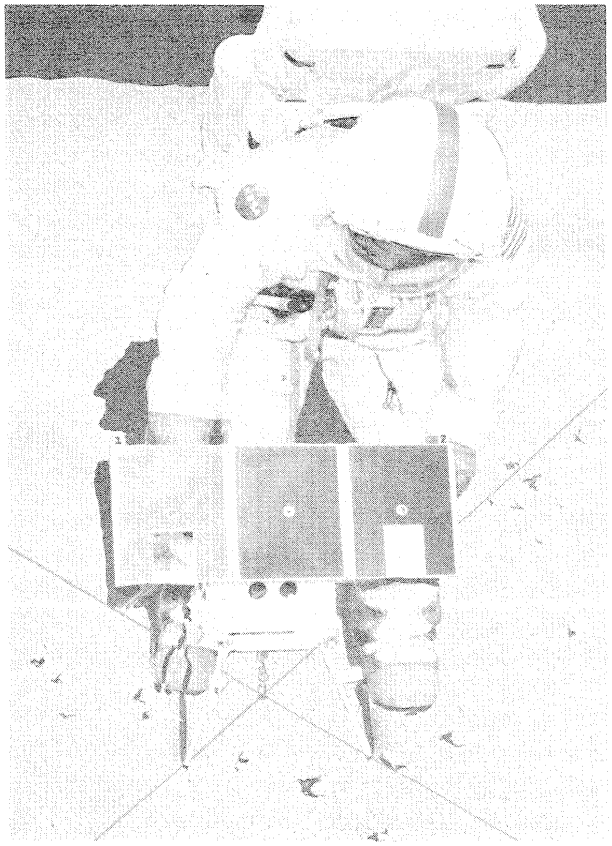

FIGURE 15-7.–The SEP experiment transmitter shown with the solar panel power source and dipole antennas deployed. The transmitter electronics package is covered on the bottom five sides with a thermal blanket. Because the top of the unit is shaded by the solar panel, the uncovered surface needs only a coat of thermal paint to provide adequate cooling for the enclosed electronics. The balance between heat lost to cold space by radiation and that generated inside the unit by the electronics equipment is very delicate and requires careful thermal design.

transmitted on the north-south (N-S) dipole antenna and received on the X antenna. In subframe 2, the receiver is calibrated at 8.1 and 4 MHz and the synchronization signal is transmitted on the east-west (E-W) antenna and received on the Y antenna. Each experiment frequency sequence is repeated exactly as shown in all six subframes. Each experiment frequency is transmitted first on the N-S antenna for 100 msec and then on the E-W antenna for 100 msec. During each 100-msec transmission interval, the receiver "looks" at the transmitted signal for a period of 33 msec with each of the three orthogonal (X,Y,Z) receiving loops. In addition to the preceding operations, once each subframe, the receiver observes environmental noise and records its amplitude.

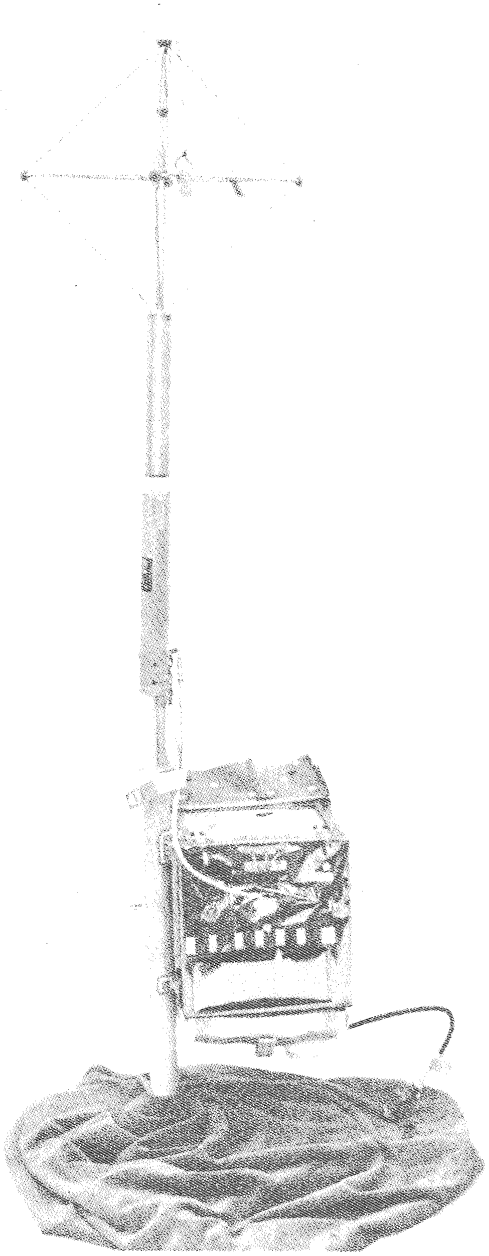

FIGURE 15-8.–The SEP experiment receiver and antennas. The receiver electronics, including tape recorder and battery, are contained in the box (23 cm^3), which usually is completely enclosed in a thermal blanket. The thermal blanket has been opened to show optical surface reflectors. The three-loop antenna assembly, folded during the journey to the Moon, is shown unfolded as it was used on the Moon.

The receiver acquires the transmitter signal sequence automatically as long as the signal exceeds a given threshold. Synchronization of the receiver is

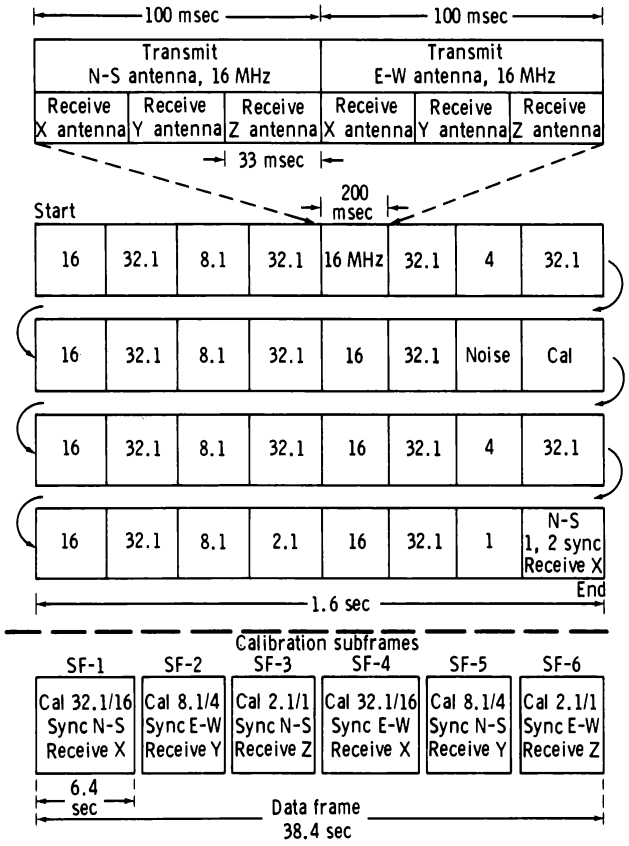

FIGURE 15-9.–The SEP experiment data format. The basic cycle, shown in the center of the diagram, starts with the 16-MHz signal and ends with the synchronization (sync) frame in the lower right corner. The cycle is 6.4 sec long. (Values are frequencies in megahertz.) The upper part of the figure shows a typical "data" frame. However, the single calibration (cal) frame changes successively through the subframe (SF) sequence shown at the bottom of the diagram.

accomplished when both (or either of) the 1- and 2.1-MHz signals exceed a given threshold. A block diagram of the SEP experiment receiver is shown in figure 15-10.

The loop antennas are connected sequentially to a low-noise amplifier section, which amplifies, converts (in frequency), and logarithmically compresses the amplitude of the received signal. A constant amplitude, variable frequency signal (in the band 300 to 3000 Hz) corresponding to the logarithm of the received signal amplitude was recorded on magnetic tape in the DSEA. The DSEA can record nearly 10 hr of data. Upon completion of the experiment, the DSEA was removed from the receiver for return to Earth.

Such functions as signal synchronization, frequency mixing, and antenna switching are controlled by the timing section, which is, in turn, crystal controlled for stability. The entire receiver assembly is battery powered using primary cells and is enclosed, except for the antenna assembly, in a thermal blanket. The thermal blanket has two flaps that may be opened to expose optical surface reflectors, which form a thermal radiator for internally produced heat while reflecting heat from the Sun, to control the internal temperature of the receiver.

The SEP experiment transmitter (figs. 15-7 and 15-11) is powered by solar cell panels that are designed to provide a minimum output of 10.0 W at 15 V and 1.10 W at 5 V. Like the receiver, the transmitter timing sequence is crystal controlled for stability. Also, separate stable crystal oscillators generate the signals that are radiated by the dipole antennas placed on the lunar surface. Because the antennas are required to radiate energy at six different frequencies, they are constructed in sections (fig. 15-12), and each section is electrically separated by electrical filters (signal traps). Each section of the antenna is of the proper electrical length for optimum performance. The dipole antennas, each 70 m long (tip to tip), are made of insulated wire between signal traps and were stored on reels until deployed.

Performance on the Lunar Surface

The crewmen deployed the SEP experiment equipment during the first period of extravehicular activity (EVA-1). Photographs of the receiver and of the transmitter and the transmitting antenna are shown in figures 15-13 and 15-14, respectively. Stereographic photographs will be used to obtain the location of the starting point of the SEP experiment profiles to within 1 m. The LRV, with its navigation system, was used to mark straight, orthogonal lines to be used as guides for deploying the antenna. Especially important for the analysis of the data was the fact that the arms of the transmitting antenna were laid out straight and at right angles to each other. The SEP experiment operations were nominal during EVA-1. During the rest period between EVA-1 and EVA-2, however, the temperature of the SEP experiment receiver increased; subsequent overheating hampered the SEP experiment operation until the DSEA recorder was removed in the middle of EVA-3 to prevent loss of data that had been recorded already

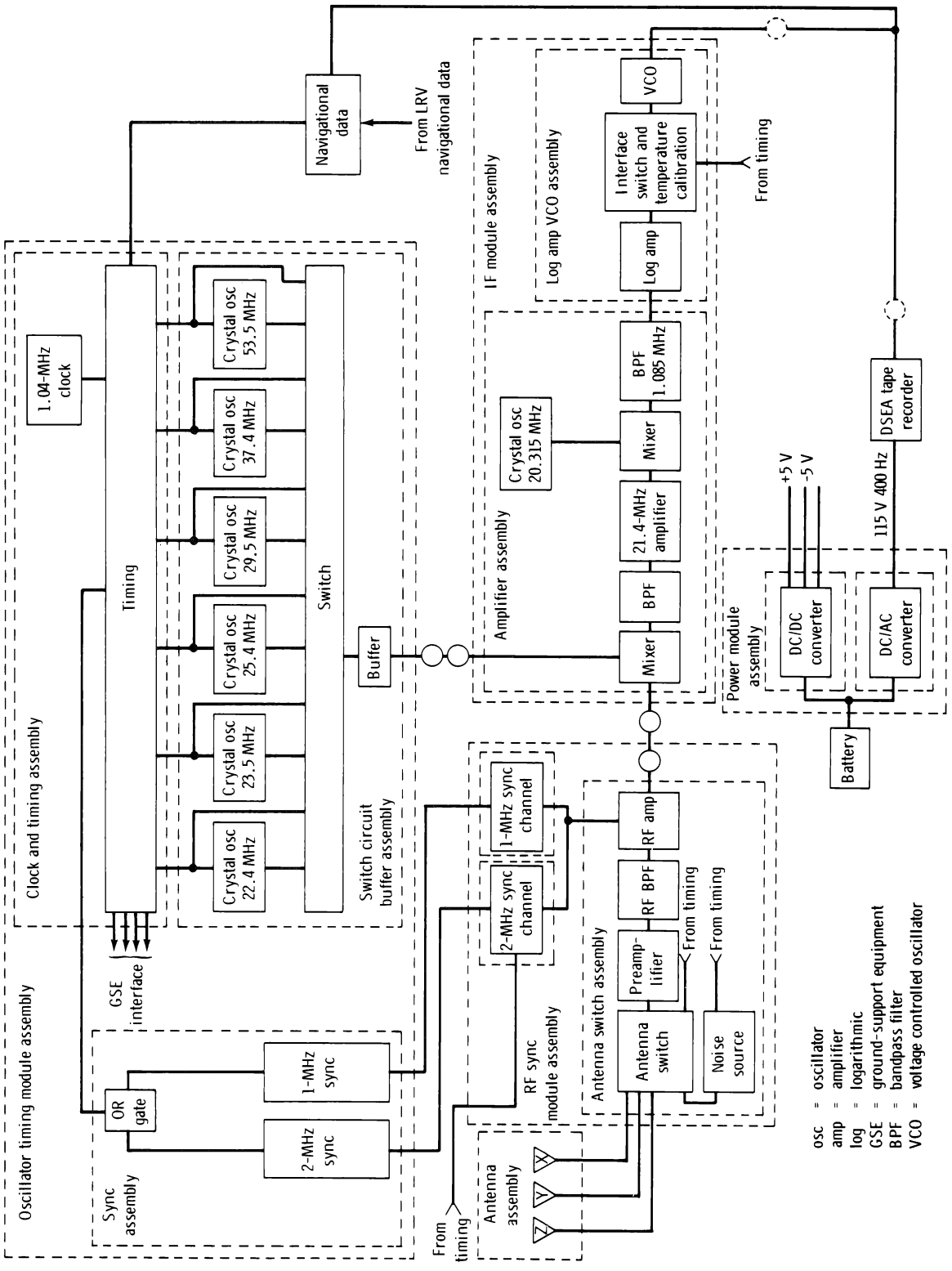

FIGURE 15-10.–Block diagram of the SEP experiment receiver.

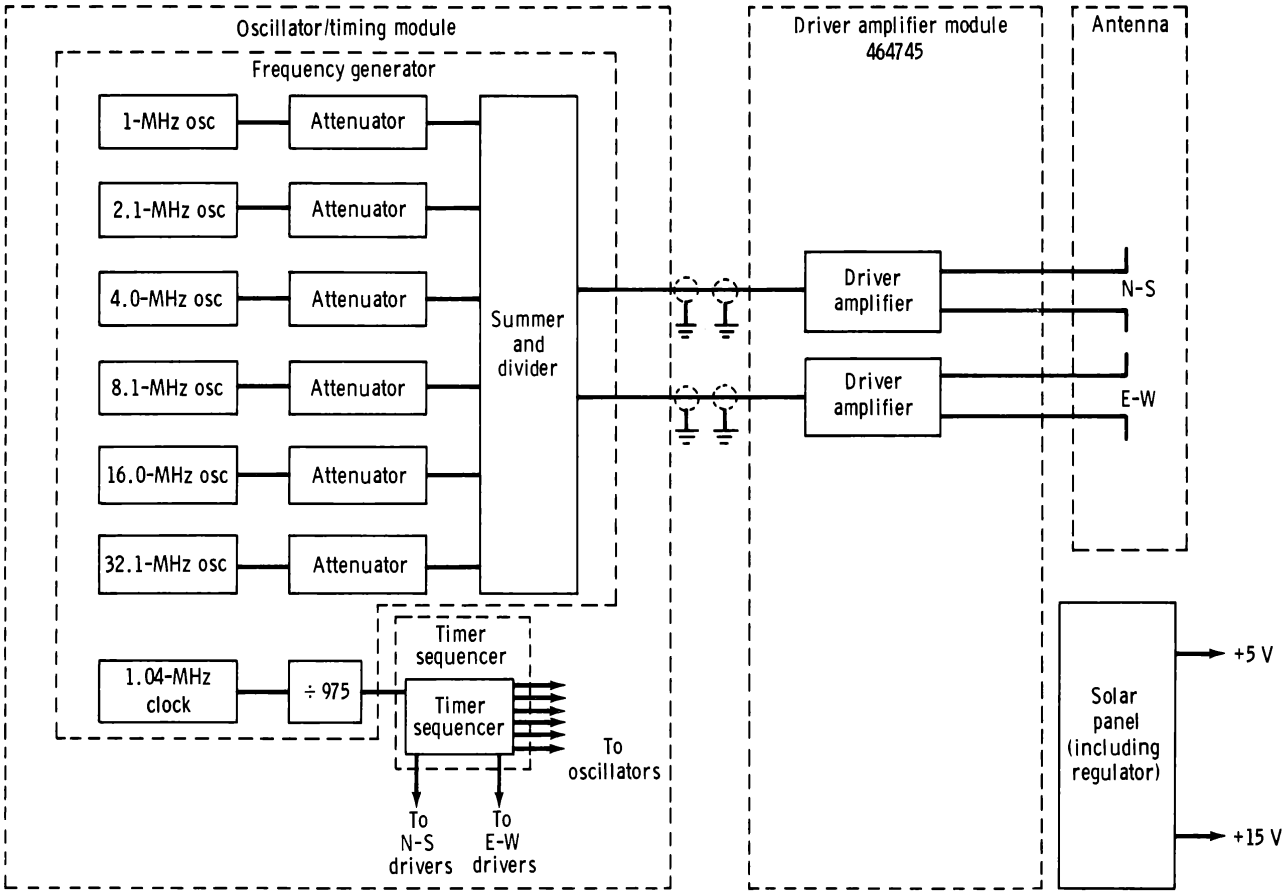

FIGURE 15-11.–Block diagram of the SEP experiment transmitter.

on the magnetic tape. The receiver contained a thermometer that was monitored by the crewmen. Despite the efforts of the crewmen to control the temperature, the receiver became too hot and was turned off by a thermally operated switch.

Data were obtained during EVA-2 on the traverses from the SEP experiment site toward station 2 and from station 4 toward the SEP experiment site. Data were not obtained during the early part of EVA-3 because the receiver switch was in the "standby" position rather than "operate." Apparently, the transmitter operated nominally throughout the mission.

THE DATA

Three kinds of data were recorded in the SEP experiment: navigational data, electromagnetic field strengths, and the internal temperature of the receiver. The navigational data, obtained from the LRV navigation system, included odometer pulses at 0.5-m increments from two wheels, the computed range to the SEP experiment transmitter in 100-m increments, and the computed bearing to the SEP experiment transmitter in 1° increments. The navigational data are approximate because of wheel slippage on the lunar surface and will be improved greatly by including additional data on the LRV location obtained from photographs, crew comments, and long-baseline interferometry.

The second kind of data, the primary SEP experiment data, consists of the three orthogonal magnetic components H_z, H_ρ, and H_ϕ, recorded as a function of frequency and of transmitting antenna (N-S or E-W). An example of the field strength data is shown in figure 15-15.

The third kind of data, temperature of the SEP experiment receiver, was obtained for use in the postflight analysis of the experiment. Because of the sensitivity of all magnetic tape to temperature, the potential loss of data from excessive temperature in the SEP experiment receiver had been anticipated. Although protection against overheating had been

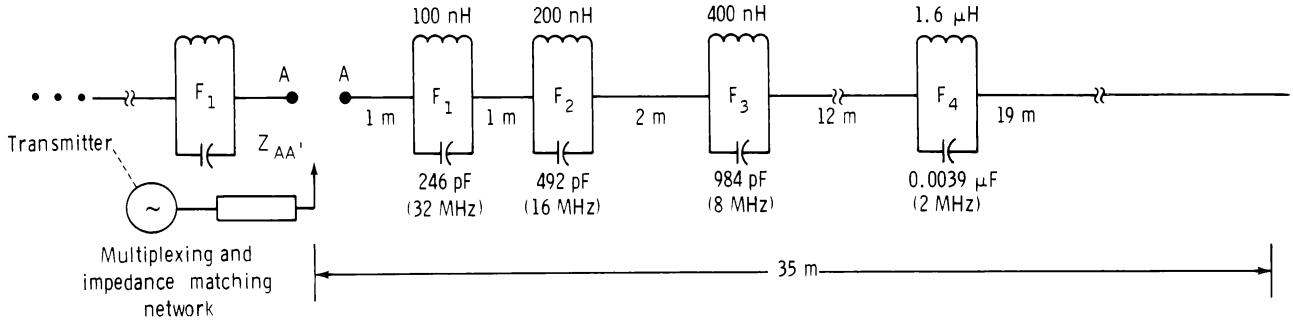

FIGURE 15-12.–Electrical schematic diagram of the SEP experiment transmitting antenna. Only one-half is shown because the antenna is symmetric about the midpoint (A′, A). Total physical length (tip to tip) of each section of the antenna used for each SEP experiment frequency is 2, 4, 8, 32, and 70 m. The symbol Z represents impedance, and the components labeled F_1 to F_4 are filters.

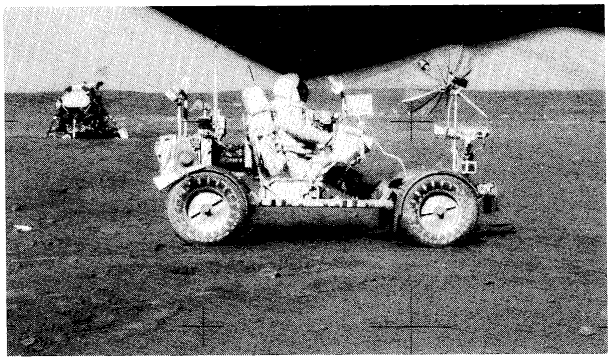

FIGURE 15-13.–The SEP experiment receiver mounted on the LRV (AS17-141-21512).

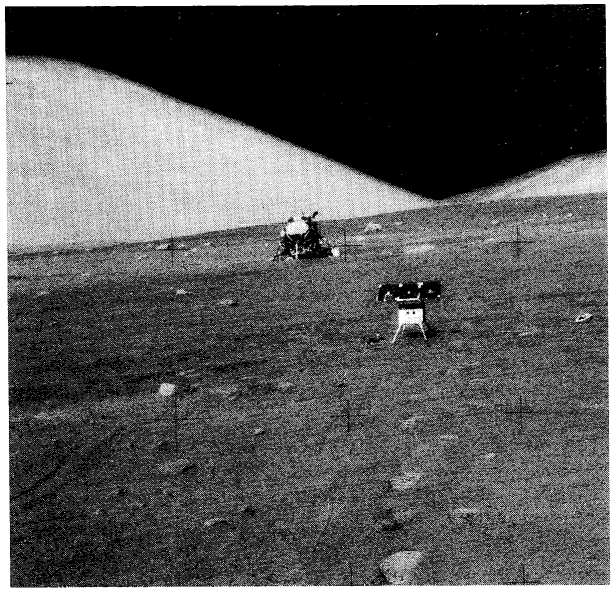

FIGURE 15-14.–The SEP experiment transmitter and antenna deployed at the Apollo 17 site (AS17-141-21517).

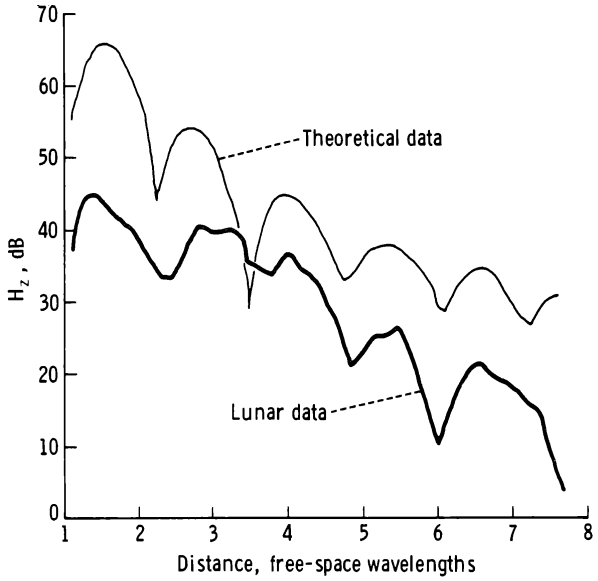

FIGURE 15-15.–Comparison of lunar data for H_z, 16-MHz, N-S transmitting antenna with the theoretical curve calculated from mode theory. Parameters are given in table 15-I.

built in, it was desired to have data on the actual temperature. A portion of the temperature curve is shown in figure 15-16.

PRELIMINARY ANALYSIS

The analysis of each individual component at each frequency for each of the transmitting antenna orientations is quite straightforward. However, a single model that fits all the data has not been found, perhaps because of the limitations of our present

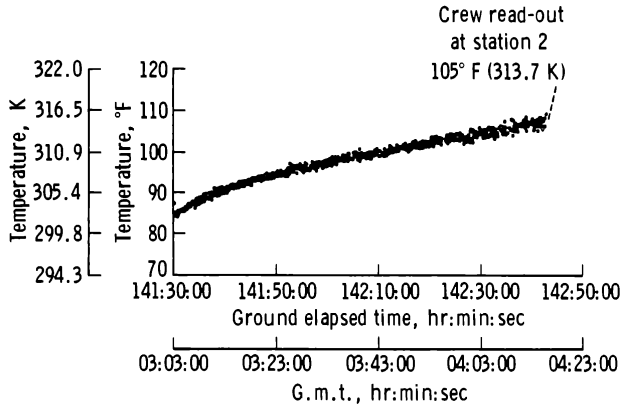

FIGURE 15-16.–Internal temperature profile of the SEP experiment receiver during the traverse from the SEP experiment site to station 2 on December 13, 1972.

TABLE 15-I.–*Preliminary Results for* H_z, *N-S Transmitting Antenna*

[p = 0.003]

Transmitter frequency, MHz	ϵ_{r_1} (a)	ϵ_{r_2} (b)	*Layer depth, m*
32.1	2.7	3.0	5.7
16	3.7	3.9	10
8.1	4.1	4.2	18
4	4.2	4.8	37
2.1	6.3	6.4	57
1	6.1	6.3	122

[a]Dielectric constant of layer.
[b]Dielectric constant of semi-infinite half space beneath layer.

theoretical development. For rigorous solutions, we are limited to models with homogeneous layers bounded by plane, horizontal surfaces. However, even within the limitations of our present theory, values of the properties of the lunar material in situ have been estimated, and some interesting conclusions about the electrical structure of the Taurus-Littrow site have been obtained.

The discussion in this report is based mainly on the analysis of H_z, the vertical component of the magnetic field, for two reasons. First, although the radiation patterns of the receiving antennas have not been measured, it is expected that the H_z data are less distorted than those of the other two components. Second, the appearance of the H_z data resembles more closely the glacier data, which comprise our background data.

Two quite different structural models of the Apollo 17 site have been developed to account for the observations. Although neither is based on rigorous theory, we believe that each is correct in the essential features. The first model, preferred by most members of the SEP experiment team, is one in which the dielectric constant increases with depth. Each of the lunar profiles can be matched quite well with the theoretical curves based on a single layer. The parameters for each of these six single-layer models are shown in table 15-I, and a typical example of the match between the theoretical and observed curves is shown in figure 15-15. The composite of these several models is shown in figure 15-17. We believe that the H_z data indicate that the dielectric constant increases with depth from a value of 2.5 to 3 near the surface to approximately 5 at a depth of 50 to 60 m. A discontinuity is present at 50 to 60 m, where ϵ_r increases to a value of 6 to 6.5. Because no reflection appears to be present in the 1-MHz data, we expect that ϵ_r does not increase between 60 m and at least 2.5 km. Compared to terrestrial values, the loss tangent is quite low (approximately 0.003) at all SEP experiment frequencies. On the basis of this low value of the loss tangent, we infer that water is probably not present at the Apollo 17 site.

In the alternate structural model, the cause of the apparent change of dielectric constant with depth is assigned to a sloping interface between a thin upper layer with $\epsilon_r = 3$ to $\epsilon_r = 4$ and $p < 0.04$ and a thick lower layer with $\epsilon_r = 6.5$ and $p = 0.04$. Rigorous theoretical expressions have not yet been obtained for this case either. However, we have confidence in the general effects attributed to a sloping interface because of the following limiting cases of horizontal interfaces.

1. For a very thin layer (thickness $< 0.1\lambda$), the interference pattern is equivalent to that of a half space in which ϵ_r and p have the values of the lower layer (fig. 15-18, upper curve).
2. For a layer with thickness between 0.1λ and 0.3λ, the individual "wiggles" of the interference pattern disappear (fig. 15-18, intermediate curves).
3. For a layer with thickness greater than approximately 0.3λ, the usual "reflected" wave appears in the pattern.

The sensitivity of the interference pattern of a thin

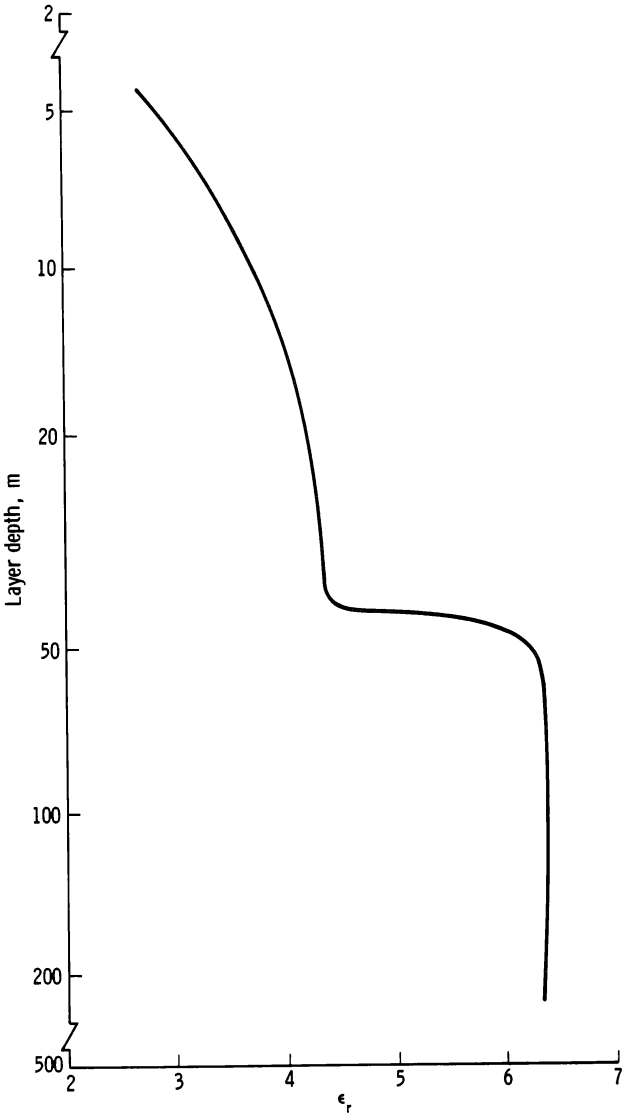

FIGURE 15-17.–Model for Apollo 17 site in which the dielectric constant varies with depth. The values of ϵ_r for each frequency are shown in table 15-I. In this figure, the approximate continuous function of ϵ_r is shown. Note that this interpretation is preliminary and, although the theoretical solution for each frequency is rigorous, the "solution" for the continuous variation of ϵ_r with depth is somewhat intuitive at present.

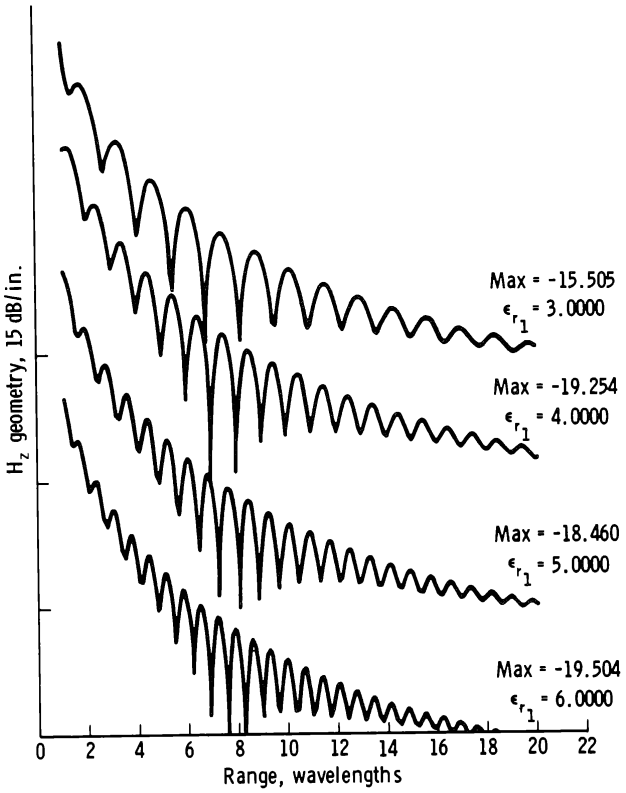

FIGURE 15-18.–Theoretical curves for thin layers, where $p_1 = 0.0300$, $\epsilon_{r_1} = 3.000$, $p_2 = 0.0400$, and $\epsilon_{r_2} = 6.000$. The points on the ordinate indicate the maximum values of each wave pattern. These plots are based on correct theory for horizontal layers, and they are used to "guess" a solution for an inclined interface.

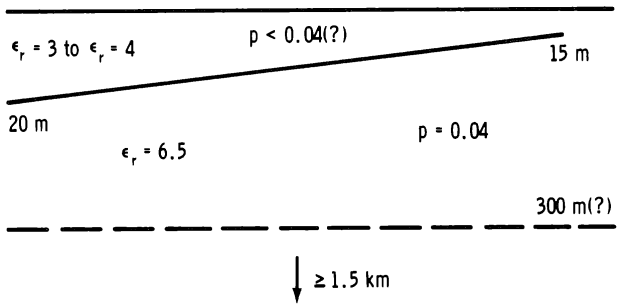

FIGURE 15-19.–The alternate model of the electrical structure at the Apollo 17 site. A layer of thickness between 0.2λ and 0.3λ is present at the SEP experiment site (left) and thins toward station 2 (right). The broken line at 300 m indicates a possible discontinuity in ϵ_r at that depth.

layer to the exact thickness is shown clearly in figure 15-18. The basis for this type of model is best seen in the 2.1-MHz profile, which resembles the intermediate theoretical curve of figure 15-18 near the SEP experiment site and resembles the upper theoretical curve of figure 15-18 farther away. The structure that best fits this analysis is shown in figure 15-19. The layer is perhaps 20 m thick beneath the SEP experiment site and thins to 15 m at station 2. In addition, there is a hint of a discontinuity in ϵ_r at a depth of approximately 300 m.

CONCLUSIONS

1. The relative dielectric constant of the lunar material at Taurus-Littrow, at frequencies of 1 to 32 MHz, is approximately 3 to 4 near the surface and increases to 6 to 7 at a depth of approximately 50 m. The loss tangent is less than 0.04 and possibly as low as 0.003.

2. The electrical structure at Taurus-Littrow is not simple horizontal layering.

3. No liquid water is present in the outer 1 to 2 km.

4. Scattering of electromagnetic waves at frequencies of 1 to 32 MHz is insignificant.

5. Continuing postflight analysis of navigational data, photographs, and other data will provide location of the LRV on the EVA-2 traverse to an accuracy of a few meters.

6. Additional theoretical and scale model work is being done to solve the problem of continuous variation with depth of the dielectric properties and the problem of dipping interface.

ACKNOWLEDGMENTS

The experiment and equipment conceptual design was done at the Massachusetts Institute of Technology Center for Space Research. The flight hardware was designed and built by the Raytheon Company.

REFERENCES

15-1. Rossiter, J. R.; LaTorraca, G. A.; Annan, A. P.; Strangway, D. W.; and Simmons, G.: Radio Interferometry Depth Sounding: Part II—Experimental Results. Geophysics, vol. 38, no. 3, June 1973, p. 581.

15-2. Sommerfeld, A.: Über die Ausbreitung der Wellen in der drahtlosen Telegraphie. Ann. Physik, vol. 28, 1909, pp. 665-737.

15-3. Baños, Alfredo, Jr.: Dipole Radiation in the Presence of a Conducting Half-Space. Vol. 9 of International Series of Monographs on Electromagnetic Waves, Pergamon Press, Inc. (New York), 1966.

15-4. Annan, A. P.: Radio Interferometry Depth Sounding. M.S. Thesis, Univ. of Toronto, 1970.

15-5. Simmons, G.; Strangway, D. W.; Bannister, L.; Baker, R.; et al.: The Surface Electrical Properties Experiment. Lunar Geophysics: Proceedings of a Conference at the Lunar Science Institute, Houston, Tex., Oct. 18-21, 1971, D. Reidel Pub. Co. (Dordrecht, Holland), 1973, pp. 258-271.

15-6. Annan, A. P.: Radio Interferometry Depth Sounding: Part I—Theoretical Discussion. Geophysics, vol. 38, no. 3, June 1973, p. 557.

15-7. Kong, J. A.: Electromagnetic Fields Due to Dipole Antennas Over Stratified Anisotropic Media. Geophysics, vol. 37, no. 6, Dec. 1972, pp. 985-996.

15-8. Tsang, L.; Kong, J. A.; and Simmons, G.: Interference Patterns of a Horizontal Electric Dipole Over Layered Dielectric Media. J. Geophys. Res., vol. 78, no. 17, June 19, 1973, pp. 3287-3300.

15-9. King, Ronold W. P.: Electromagnetic Engineering, Vol. I—Fundamentals. McGraw-Hill Book Co., Inc. (New York), 1945.

15-10. Jordan, Edward C.; and Balmain, Keith G.: Electromagnetic Waves and Radiating Systems. Second ed., Prentice-Hall, Inc. (Englewood Cliffs, N.J.), 1968.

15-11. Stratton, Julius Adams: Electromagnetic Theory. McGraw-Hill Book Co., Inc. (New York), 1941.

15-12. Smythe, W. R.: Static and Dynamic Electricity. McGraw-Hill Book Co., Inc. (New York), 1950.

15-13. Lorrain, Paul; and Corson, Dale R.: Electromagnetic Fields and Waves. W. H. Freeman (San Francisco), 1970.

15-14. Pierce, G. W.: A Table and Method of Computation of Electric Wave Propagation, Transmission Line Phenomena, Optical Refraction, and Inverse Hyperbolic Functions of a Complex Variable. Proc. Am. Acad. Arts Sciences, vol. 57, 1922, p. 175.

15-15. Galejs, Janis: Antennas in Inhomogeneous Media. Vol. 15 of International Series of Monographs on Electromagnetic Waves, Pergamon Press, Inc. (New York), 1969.

15-16. Wait, James R.: Electromagnetic Waves in Stratified Media. Vol. 3 of International Series of Monographs on Electromagnetic Waves, Pergamon Press, Inc. (New York), 1962.

15-17. Brekhovskikh, Leonid M. (David Lieberman, trans.): Waves in Layered Media. Vol. 6 of Applied Mathematics and Mechanics, Academic Press (New York), 1960.

15-18. Sommerfeld, A.: Über die Ausbreitung der Wellen in der drahtlosen Telegraphie. Ann. Physik, vol. 81, 1926, pp. 1135-1153.

15-19. Tsang, Leung: Electromagnetic Near Fields of Horizontal Dipole on Stratified Lunar Surface. B.S. Thesis, Mass. Inst. of Tech., 1971.

15-20. Strangway, D. W.; Simmons, G.; Watts, R.; LaTorraca, G.; et al.: Radio Frequency Interferometry—A New Technique for Studying Glaciers. J. Glaciology, vol. 12, 1973.

15-21. LaTorraca, Gerald A.: Half Wavelength Dipole Antennas Over Stratified Media. NASA CR-115561, 1972.

15-22. Simmons, Gene; Meyer, James W.; Baker, Richard H.; and Strangway, David W.: Brief Introduction to the Surface Electrical Properties Experiment. MIT Press (Cambridge, Mass.), Aug. 1972.